Acadlore Transactions on Geosciences
https://www.acadlore.com/journals/ATG

Reassessing the Water Invasion Intensity Indicator Curve and Endpoint Equation in Water-Drive Gas Reservoirs

Shaopeng Zhu, Xiaodong Peng*, Yuqiang Zha, Chunjun Hu, Cheng Guo

CNOOC China Limited, Hainan Branch, 570311 Haikou, China

* Correspondence: Xiaodong Peng (41294776@qq.com)

Received: 08-05-2024 **Revised:** 09-10-2024 **Accepted:** 09-20-2024

Citation: S. Zhu, X. Peng, Y. Zha, C. Hu, C. Guo, "Reassessing the water invasion intensity indicator curve and endpoint equation in water-drive gas reservoirs," *Acadlore Trans. Geosci.*, vol. 3, no. 3, pp. 161–172, 2024. https://doi.org/10.56578/atg030304.

Abstract: The traditional view that the production indicator curve of water-drive gas reservoirs exhibits an upward trend is not entirely consistent with production practices. Additionally, the classical method of calibrating gas recovery using the water invasion intensity indicator curve in conjunction with the endpoint equation has shown limited applicability. To address these issues, a material balance-based dynamic prediction approach that accounts for water production was employed in this study. Both the Carter-Tracy unsteady-state model and the Schithuis steady-state model were used to calculate water invasion volumes, followed by a sensitivity analysis of the factors influencing the production indicator curve of water-drive gas reservoirs. A reassessment of the water invasion intensity indicator curve, the endpoint equation, and gas recovery in water-drive gas reservoirs was conducted, and the findings were validated using field production data from a typical reservoir. The results indicate that (a) When water production is considered, the overall production indicator curve of water-drive gas reservoirs exhibits a smooth convex shape, intersecting the cumulative gas production axis at the dynamic reserves point. The early-stage characteristics may appear as an upward trend, an approximately linear segment, or a downward bend. (b) The water invasion intensity indicator curve is only applicable for short-term predictions in the early development stage. It is more suitable for strongly water-driven gas reservoirs under steady-state conditions. The endpoint equation may vary depending on different aquifer conditions and development scenarios. (c) The larger the aquifer radius, the higher the aquifer permeability (i.e., the greater the water invasion index), the greater the compressibility coefficients of the rock and formation water, the lower the gas production rate, the deeper the gas reservoir burial depth, the more pronounced the convexity of the dimensionless production indicator curve, the higher the abandonment pressure, and the lower the gas recovery. These findings provide insights into the production indicator curve and recovery of water-drive gas reservoirs, which align with production practices, offering valuable guidance for development patterns, recovery calibration, and enhanced recovery techniques.

Keywords: Water-drive gas reservoirs; Gas production indicator curve; Water invasion intensity indicator curve; Endpoint equation; Material balance dynamic prediction; Gas recovery; Sensitivity analysis

1 Introduction

The material balance equation for gas reservoirs can be expressed in two forms: the pseudo-pressure form and the apparent geological reserves form [1]. In 2002, Li [2] defined the relationship curve between pseudo-pressure (p/z) and cumulative gas production (Gp) as the gas reservoir production indicator curve and provided a comparative schematic of the production indicator curves for constant volume, closed, and water-drive gas reservoirs. For water-drive gas reservoirs, Dake [3], Ahmed [4], John Robert and Wouter Ehrenberg [5], Elahmady and Wattenbarger [6], and Ezekwe [7] summarized schematic representations of typical gas reservoir production indicator curves under different aquifer energy conditions. Extensive sensitivity quantitative analyses of production indicator curves in water-drive gas reservoirs have been conducted [8–18]. In 1998, Zhang and Li [8] derived a set of upward dimensionless production indicator curves based on the empirical relationship between water storage volume coefficient and recovery degree, defining them as water invasion intensity indicator curves. In 1999, Liu et al. [9] developed a method to predict the future water invasion volume and reservoir pressure using the unsteady-state water invasion volume and the material balance equation for water-drive gas reservoirs. In 2005, Sheng and Li [10] employed

numerical simulation to analyze the impact of gas production rate and aquifer size on the production dynamics of sandstone bottom-water gas reservoirs. In 2011, Spivy [11] obtained gas reservoir production indicator curves for various typical aquifers through pressure response calculations under different water invasion models and gas field production methods. In 2015, Li et al. [12] investigated the factors influencing gas recovery in water-drive gas reservoirs by integrating the material balance equation with the endpoint equation.

In 2016, Lu [13] combined the material balance equation for water-drive gas reservoirs with the Fetkovich analytical aquifer model and employed a trial method to analyze the applicability of the water invasion intensity indicator curve. In 2017, Yang et al. [14] conducted a series of sensitivity analyses based on the production indicator curve of the YC13-1N gas reservoir, leading to a reassessment of the production indicator curves for both water-drive and abnormally high-pressure gas reservoirs. In 2018, Peng et al. [15] proposed a novel method for calculating dynamic reserves in gas reservoirs with finite closed aquifers. In 2020, Peng et al. [16] performed material balance simulations on a typical abnormally high-pressure water-drive gas reservoir in the western South China Sea, and the findings were validated through long-core depletion experiments, providing a new understanding of water-drive production indicator curves. In 2021, Peng et al. [17] conducted a statistical analysis of gas recovery in numerous water-drive gas reservoirs in the western South China Sea, leading to the development of a revised understanding of gas recovery and new strategies for reservoir development. In this study, based on the material balance-based dynamic prediction method that accounts for water production, the Carter-Tracy unsteady-state and Schithuis steady-state water invasion volume computing models were utilized, along with a constant gas production rate prediction approach. Relative permeability curves were incorporated to predict water production. A sensitivity analysis was conducted to examine the factors influencing the production indicator curve in water-drive gas reservoirs. The water-drive gas reservoir production indicator curve, water invasion intensity indicator curve, endpoint equation, and gas recovery were reassessed. Finally, the newly derived insights were validated using production data from a typical gas reservoir.

2 Issues with the Water Invasion Intensity Curve

The material balance equation for gas reservoirs in the pseudo-pressure form [1] is expressed as:

$$\frac{p}{z}\left(1-E_{\mathrm{p}}-\omega\right)=\frac{p_{\mathrm{i}}}{z_{\mathrm{i}}}\left(1-\frac{G_{\mathrm{p}}}{G}\right)\Omega(\mathrm{fj}) \tag{1}$$

$\omega=\frac{W_{\mathrm{e}}-W_{\mathrm{p}}B_{\mathrm{w}}}{GB_{\mathrm{gi}}}$ is the water storage volume coefficient (dimensionless); G is the dynamic gas reserves $\left(10^8\ \mathrm{m}^3\right)$; G_{p} is the cumulative gas production $\left(10^8\ \mathrm{m}^3\right)$; W_{e} is the cumulative water intrusion $\left(10^8\ \mathrm{m}^3\right)$; W_{p} is the cumulative water production $\left(10^8\ \mathrm{m}^3\right)$; p is the formation pressure (MPa); p_{i} is the initial formation pressure (MPa); z is the gas deviation factor (dimensionless); z_{i} is the gas deviation factor at initial formation pressure (dimensionless); B_{w} is the formation water volume coefficient (dimensionless); B_{gi} is the gas formation volume factor at initial formation pressure (dimensionless); C_{w} is the formation water compressibility coefficient $\left(\mathrm{MPa}^{-1}\right)$; C_{p} is the formation rock compressibility coefficient $\left(\mathrm{MPa}^{-1}\right)$; and S_{wi} is the irreducible water saturation (dimensionless).

The water invasion intensity indicator curve was proposed by Zhang and Li [8] in 1998 using an empirical formula under the assumption that the compressibility coefficients of rock and formation water are negligible.

Let

$$R_{\mathrm{g}}=\frac{G_{\mathrm{p}}}{G} \tag{2}$$

where, $f(x)$ = $f(m-1)(x)$ and L is the loss of function.

Zhang and Li [8] suggested that a functional relationship must exist between the water storage volume coefficient (ω) and the recovery degree (R_{g}), and that this function is inherently related to water invasion intensity, expressed as:

$$\omega=R_{\mathrm{g}}^{B} \tag{3}$$

where, B is a dimensionless parameter characterizing water invasion intensity; the smaller its value, the stronger the water invasion, and vice versa. When $B=1, \omega=R_{\mathrm{g}}$, indicating a rigid water drive. When $B\to\infty, \omega\to 0$, indicating that no water invasion has occurred and the reservoir behaves as a purely elastic gas drive system. When $0<B<\infty$, the reservoir is classified as a general water-drive gas reservoir (Figure 1).

By substituting Eq. (3) into Eq. (1), neglecting E_{p} of the water-drive gas reservoir, and defining the following:

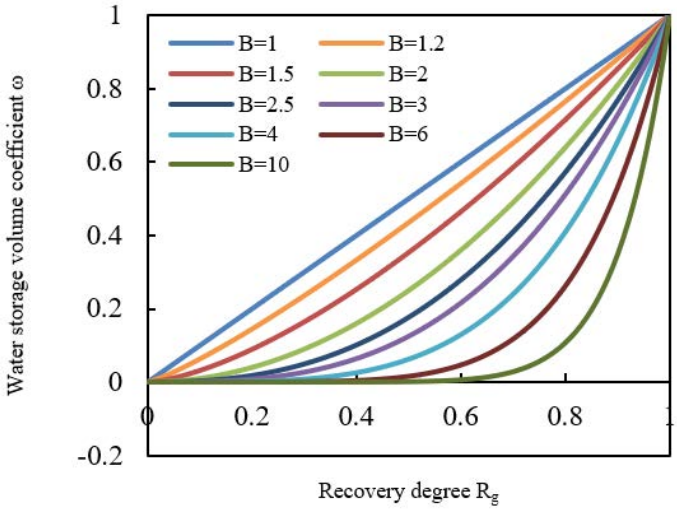

Figure 1. Relationship between recovery degree and water storage volume coefficient under different water invasion intensities [8]

$$\psi = \left(\frac{p}{z}\right) / \left(\frac{p_{\mathrm{i}}}{z_{\mathrm{i}}}\right) \tag{4}$$

The following expression is obtained:

$$\psi = \frac{1 - R_{\mathrm{g}}}{1 - R_{\mathrm{g}}^{B}} \tag{5}$$

Based on Eq. (5), different values of B can be assumed to generate a set of theoretical curves reflecting the relationship between recovery degree and dimensionless pseudo-pressure under various water invasion intensities. These curves constitute the water invasion intensity indicator curves (Figure 2).

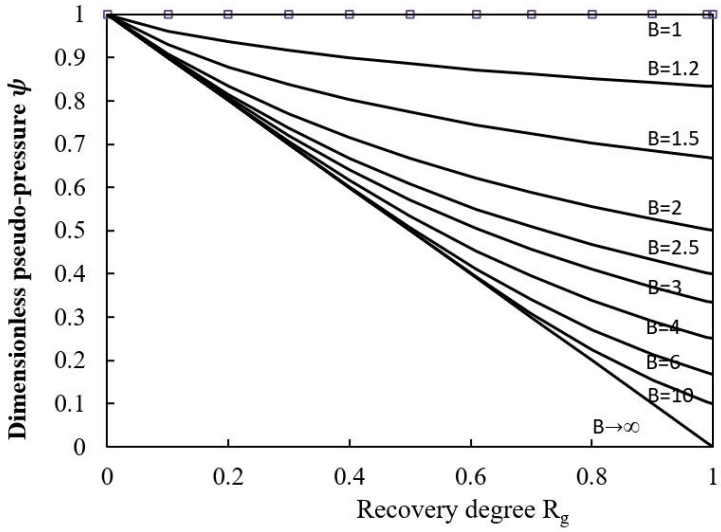

Figure 2. Relationship between recovery degree and the dimensionless curve under different water invasion intensities [8]

In 1965, Agarwal et al. [18] proposed, based on the principle of material balance, that the maximum recoverable reserves of a water-drive gas reservoir are equal to the original gas in place minus the volume of residual gas trapped

in the invaded region and the volume of remaining gas in uninvaded zones that cannot be produced. This relationship is expressed as the endpoint equation (Eq. 6):

$$P_{\mathrm{D}} = \frac{1 - R_{\mathrm{g}}}{1 - (1 - S_{\mathrm{gr}}/S_{\mathrm{gi}})\, E_{\mathrm{Va}}} \tag{6}$$

where, P_{D} is the dimensionles $_{\mathrm{s}}$ abandonment pseudo-pressure; S_{gr} is the residual gas saturation (fraction); S_{gi} is the initial gas saturation (fraction); and E_{Va} is the water-drive sweep efficiency at abandonment conditions (fraction).

Theoretically, the dimensionless abandonment pseudo-pressure (P_{D}) is a linear function of gas recovery (R_{g}), and the corresponding relationship curve is referred to as the endpoint curve. The classical method of calibrating gas recovery in water-drive gas reservoirs combines the water invasion intensity indicator curve with the endpoint equation and is widely applied [12]. Based on the graphical solution approach, the intersection of the water invasion intensity indicator curve and the endpoint curve determines the gas recovery and abandonment formation pressure of water-drive gas reservoirs (Figure 3).

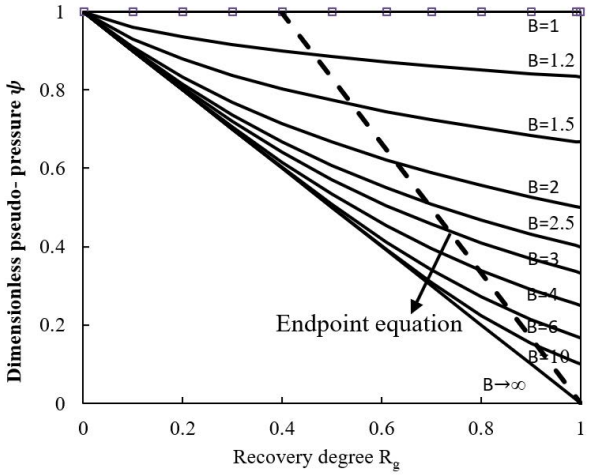

Figure 3. Relationship between water invasion intensity curves and the endpoint equation

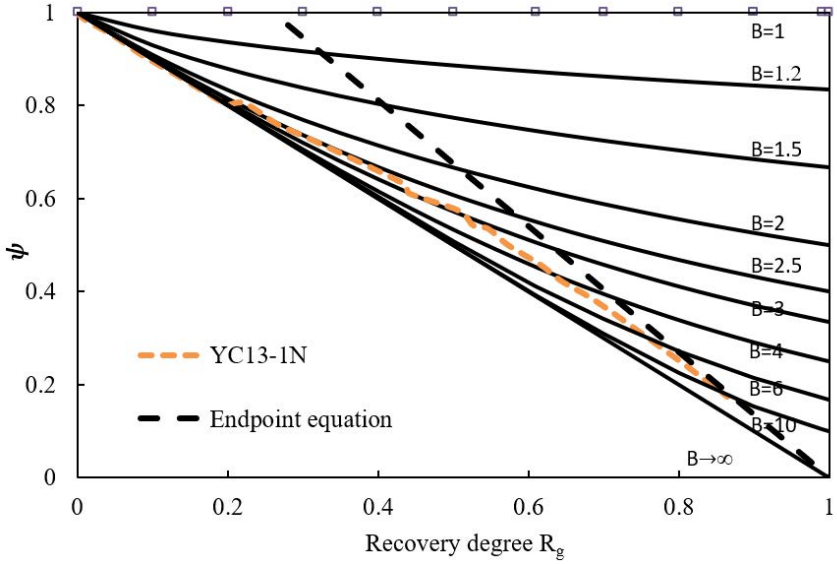

Figure 4. Dimensionless production indicator curve of the YC13-1-N gas reservoir

However, production data from typical gas reservoirs in the western South China Sea indicate that the dimensionless production indicator curves of these reservoirs do not fully align with the water invasion intensity indicator curves. Taking YC13-1, the first high-yield offshore gas field in China, as an example, this reservoir is a closed edge-water gas reservoir controlled by fault blocks, lithology, and stratigraphy within a normal pressure system. The

aquifer size is approximately three to five times that of the gas reservoir. The formation temperature is $176.1^{\circ}\mathrm{C}$, and the initial formation pressure is 38.54 MPa . Structurally, the reservoir is segmented by faults into three blocks: S, N, and NT. The primary reservoir consists of braided river delta sandstones from the third member of the Ling Formation, which were influenced by tidal processes. Well logging interpretations indicate an average porosity of 12.9% and an average permeability of $370 \times 10^{-3} \mu\ \mathrm{m}^2$, classifying it as a low-porosity, medium-permeability to medium-porosity, high-permeability reservoir [14]. However, the production indicator curve for the N block exhibits a smooth downward curvature rather than an upward trend, which contradicts the water invasion intensity indicator curve templates (Figure 4). Based on calculations of dynamic reserves and water invasion volume, a variable capacity and water invasion correction was applied to the production indicator curve. The corrected results indicate that the downward curvature is essentially a convex shape, primarily due to the energy supplementation from water invasion [14].

3 Sensitivity Analysis of the Water Invasion Intensity Indicator Curve

3.1 Material Balance-Based Dynamic Prediction Method for Water-Drive Gas Reservoirs

The fundamental equations required for material balance-based dynamic prediction in water-drive gas reservoirs include the material balance equation for water-drive gas reservoirs, the water invasion volume calculation equation, relative permeability curves, and high-pressure fluid property parameters [16, 17].

a) The material balance equation for water-drive gas reservoirs is expressed as follows [1]:

$$G\left(B_{\mathrm{g}}-B_{\mathrm{gi}}\right)+GB_{\mathrm{gi}}\left(\frac{C_{\mathrm{w}}S_{\mathrm{wi}}+C_{\mathrm{p}}}{1-S_{\mathrm{wi}}}\right)\left(p_{\mathrm{i}}-p\right)+W_{\mathrm{e}}=G_{\mathrm{p}}B_{\mathrm{g}}+W_{\mathrm{p}}B_{\mathrm{w}} \tag{7}$$

where, B_{g} is the gas formation volume factor $\left(\mathrm{m}^3/\mathrm{m}^3\right)$.

b) Cumulative water invasion volume calculation equation

For water invasion volume calculations, the Carter-Tracy unsteady-state model and the Schithuis steady-state model, both based on a planar radial flow configuration, were selected.

The cumulative water invasion volume equation for the Carter-Tracy model is given as follows [4, 19]:

$$W_{\mathrm{en}}=W_{\mathrm{en-1}}+\left(t_{\mathrm{Dn}}-t_{\mathrm{Dn-1}}\right)\left[\frac{C\Delta p_{\mathrm{n}}-W_{\mathrm{en-1}}p'_{\mathrm{D}}\left(t_{\mathrm{Dn}}\right)}{p_{\mathrm{D}}\left(t_{\mathrm{Dn}}\right)-t_{\mathrm{Dn-1}}p'_{\mathrm{D}}\left(t_{\mathrm{Dn}}\right)}\right] \tag{8}$$

where, n and n-1 represent the n-th and $(n-1)$-th time steps, respectively; C is the water invasion constant $\left(\mathrm{m}^3/\mathrm{MPa}\right)$; Δp_{n} is the pressure change at each time step (MPa); t_{D} is the dimensionless time; p_{D} is the dimensionless pressure; and p'_{D} is the derivative of dimensionless pressure.

The water invasion volume equation for the Schithuis steady-state model is expressed as [4, 19]:

$$W_{\mathrm{e}}=J_{\mathrm{w}}\int_{0}^{t}\left(p_{\mathrm{i}}-p\right)dt \tag{9}$$

where, J_{w} is the water invasion constant $\left(\mathrm{m}^3/\mathrm{d}/\mathrm{MPa}\right)$; and t is time (d).

c) Water production volume equation

Water production volume was calculated using the relative permeability curve and the fractional flow equation, expressed as follows [1]:

$$f_{\mathrm{w}}=\frac{1}{1+\frac{\mu_{\mathrm{w}}}{\mu_{\mathrm{g}}}\cdot\frac{k_{\mathrm{rg}}}{k_{\mathrm{rw}}}} \tag{10}$$

where, f_{w} is the water cut (fraction); μ_{w} and μ_{g} are the viscosities of formation water and natural gas, respectively $(\mathrm{mPa}\cdot\mathrm{s})$; k_{rw} and k_{rg} are the relative permeabilities of formation water and natural gas, respectively (fraction).

d) High-pressure property equation

The gas formation volume factor, gas deviation factor, and viscosity were determined using empirical formulas constrained by experimental results.

e) Prediction approach

Since the objective of this study is to investigate the theoretical characteristics of gas reservoir production indicator curves, material balance-based dynamic prediction was performed under a constant gas production rate. The effects of wellbore flow, abandonment pressure, and gathering and transportation pressure were not considered.

3.2 Fundamental Parameters for Dynamic Prediction

Material balance-based dynamic prediction, considering water production conditions, was conducted for the Y gas field using the material balance (MBAL) module of the IPM software. The gas reservoir parameters are presented in Table 1, the relative permeability curves are shown in Figure 5, and the sensitivity parameter design is listed in Table 2 and Table 3.

Table 1. Fundamental parameters for material balance-based dynamic prediction of the Y gas field [16, 17]

Parameter	Value
Reservoir burial depth $(H)(\mathrm{m})$	3193.3
Initial formation pressure (p_{i}) (MPa)	53.210
Initial formation temperature (T) $(^{\circ}\mathrm{C})$	152.43
Formation pressure coefficient (α)	1.682
Geothermal gradient (G_{T}) $\left(^{\circ}\mathrm{C}\cdot\mathrm{km}^{-1}\right)$	39.8
Porosity (φ)	0.178
Permeability (k) $\left(10^{-3}\mu\ \mathrm{m}^2\right)$	13.5
Initial water saturation (S_{wi})	0.495
Formation water compressibility (C_{w}) $\left(10^{-4}\mathrm{MPa}^{-1}\right)$	5.58
Pore compressibility of formation rock (C_{p}) $\left(10^{-4}\mathrm{MPa}^{-1}\right)$	5.34
Gas relative density (γ_{g})	0.645
Gas formation volume factor at initial formation pressure (B_{g}) $\left(10^{-3}\ \mathrm{m}^3\cdot\ \mathrm{m}^{-3}\right)$	3.389
Gas deviation factor at initial formation pressure (z_{i})	1.226
Original gas in place (G) $\left(10^8\ \mathrm{m}^3\right)$	344.72

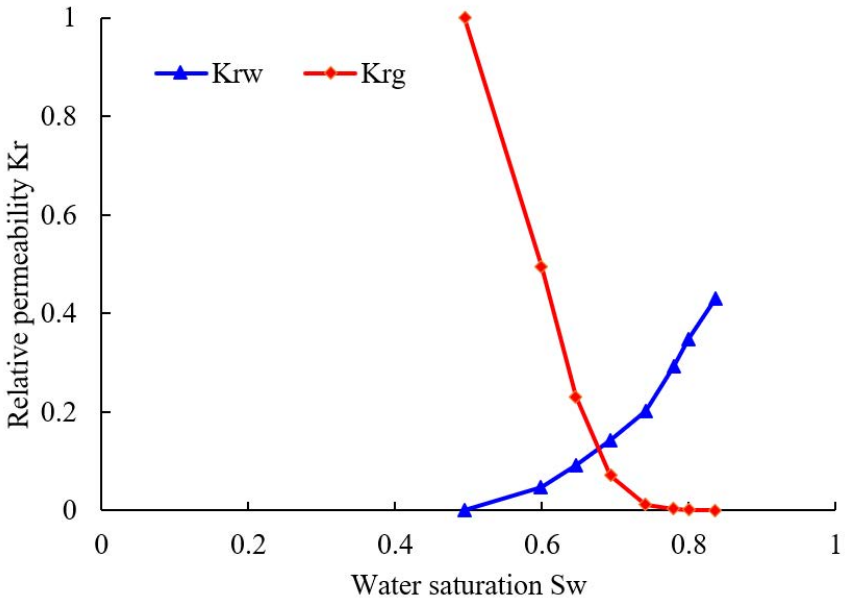

Figure 5. Relative permeability curve of the Y gas field [16, 17]

3.3 Analysis of Dynamic Prediction Results

a) As shown in Figure 6, the predicted production indicator curve of the gas reservoir, when considering water production, initially exhibits an upward trend before bending downward. After bending downward, the curve transitions into an approximately linear shape, maintaining an overall convex characteristic. The inflection point corresponds to the onset of water production. Eventually, the curve intersects the cumulative gas production axis at $G_{\mathrm{p}} = G$, where $p/zG_{\mathrm{p}} = G$=0.

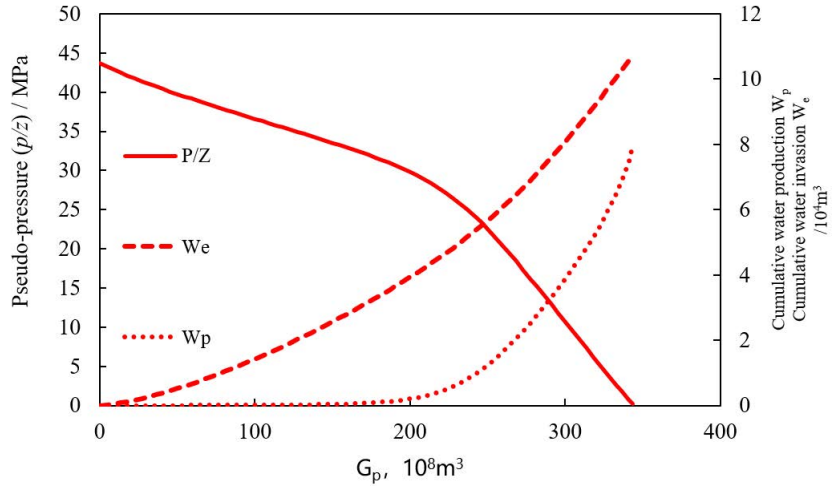

(a)

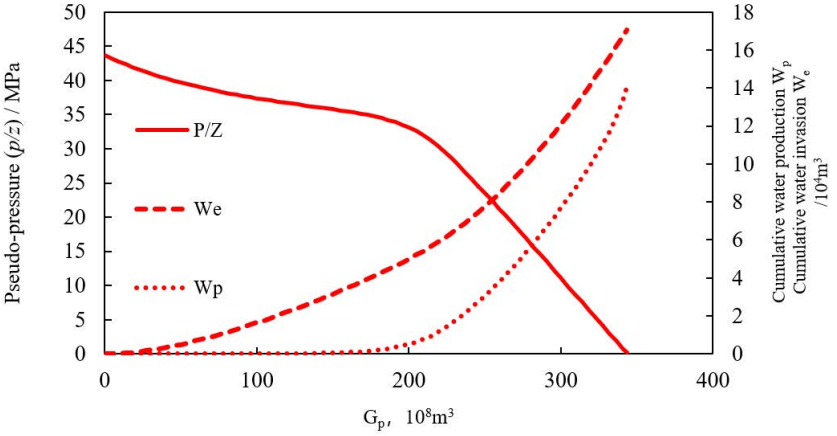

(b)

Figure 6. Material balance-based dynamic prediction results for the Y gas field (a) Carter-Tracy aquifer $\left(k = 13.5 \times 10^{-3}\mu\ \mathrm{m}^2, R_{\mathrm{D}} = 5\right)$; (b) Schithuis steady-state aquifer $\left(J_{\mathrm{w}} = 13.24\ \mathrm{m}^3/(\mathrm{d}\cdot\mathrm{MPa})\right)$

Table 2. Sensitivity parameters and their values for the Y gas field (Carter-Tracy model) [16, 17]

Sensitivity Parameter	Value
Ratio of aquifer radius to gas reservoir radius (R_{D})	$1, 2, 3, 5, 10$
Multiplication factor of aquifer permeability (K_{wD})	$0.1, 1, 10, 20, 50$
Multiplication factor of formation water compressibility (C_{wD})	$0.1, 1, 5, 10, 20$
Multiplication factor of formation rock pore compressibility (C_{pD})	
Gas production rate $(Q_{\mathrm{g}})\,(\%)$	$2.4, 4.8, 9.6, 23.9, 47.9$
Reservoir burial depth $(H)(\mathrm{m})$	$500, 1000, 2000, 3193, 4000$

b) As shown in Figure 7, the dimensionless production indicator curves of the gas reservoir, based on the Carter-Tracy water invasion model and considering water production, exhibit a smooth convex shape and ultimately intersect the cumulative gas production axis at the dynamic reserves point, where $\psi\,(R_{\mathrm{g}} = 1) = 0$. The larger values of the aquifer radius, aquifer permeability, rock compressibility, formation water compressibility, and reservoir burial depth, the lower the gas production rate, the more pronounced the convex shape in the dimensionless production indicator curve, the more distinct the upward trend in the early stage, the smaller the recovery factor (R_{g}) at the inflection point, and the longer the linear trend after the downward bending phase in the later stage.

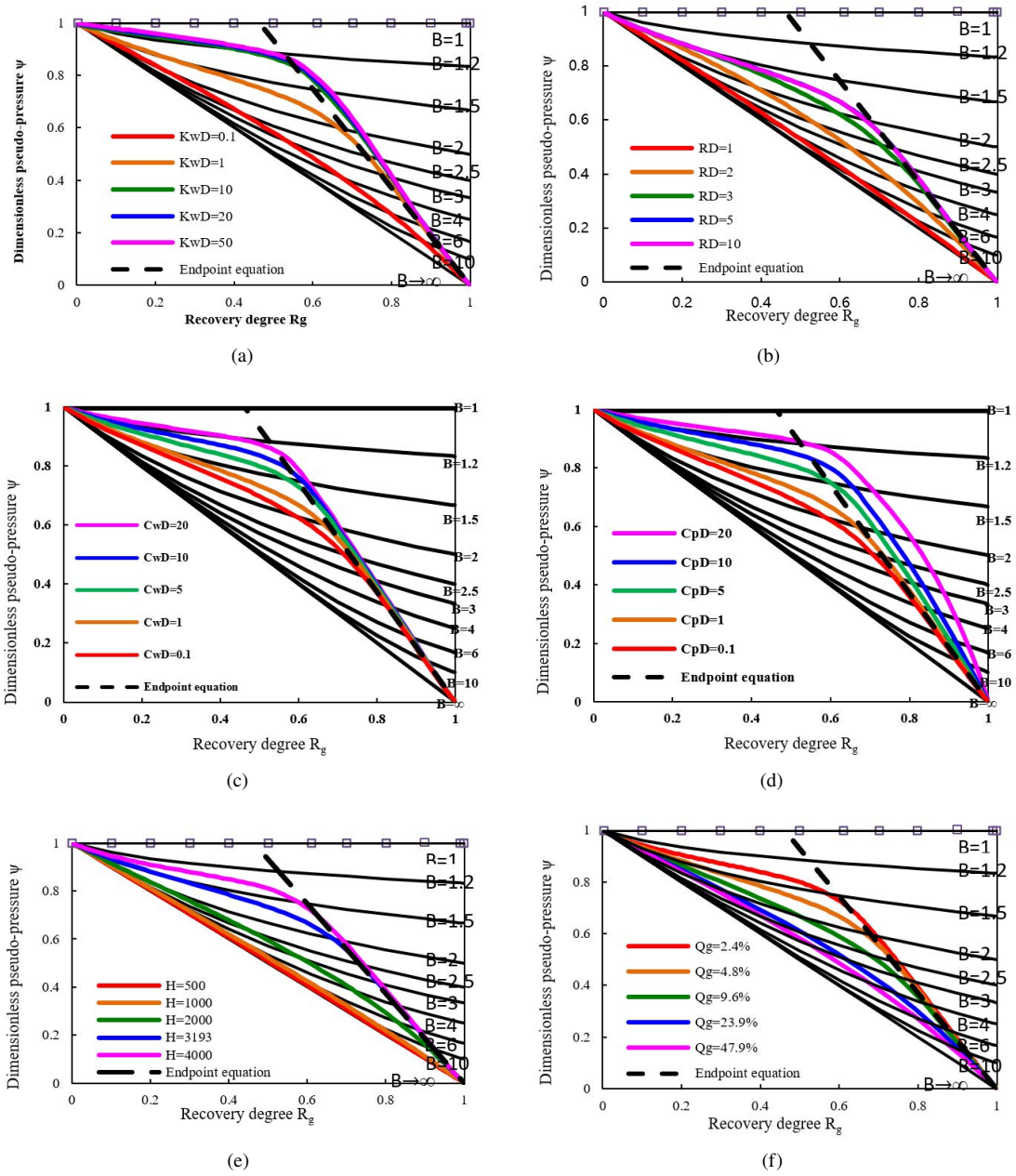

Figure 7. Dimensionless production indicator curves and water invasion intensity indicator curves (a) Aquifer permeability; (b) Aquifer radius; (c) Formation water compressibility; (d) Formation rock pore compressibility; (e) Reservoir burial depth; (f) Gas production rate

Table 3. Sensitivity parameters for material balance-based dynamic prediction of the Y gas field (Schithuis model) [16, 17]

Parameter	Value
Steady-state water invasion index (J_{w}) $\left(\mathrm{m}^3 \cdot \mathrm{d}^{-1} \cdot \mathrm{MPa}^{-1}\right)$	$0, 1.32, 6.62, 13.24, 132.42$
Gas production rate $(Q_{\mathrm{g}})\,(\%)$	$2.4, 4.8, 9.6, 23.9, 47.9$
Reservoir burial depth $(H)(\mathrm{m})$	$500, 1000, 2000, 3193, 4000$

c) As shown in Figure 8, the dimensionless production indicator curves of the gas reservoir, derived from the Schithuis water invasion model while considering water production, also exhibit an overall smooth convex shape and ultimately intersect the cumulative gas production axis at the dynamic reserves point, where $\psi\left(R_{\mathrm{g}}=1\right)=0$.

However, these curves demonstrate an initial upward trend followed by a downward bend, transitioning into a linear pattern in the later stage. The larger the values of the water invasion index and reservoir burial depth, the lower the gas production rate, the more pronounced the convex shape in the dimensionless production indicator curve, the more distinct the upward trend in the early stage, the smaller the recovery factor (R_{g}) at the inflection point, and the longer the linear trend after the downward bending phase in the later stage.

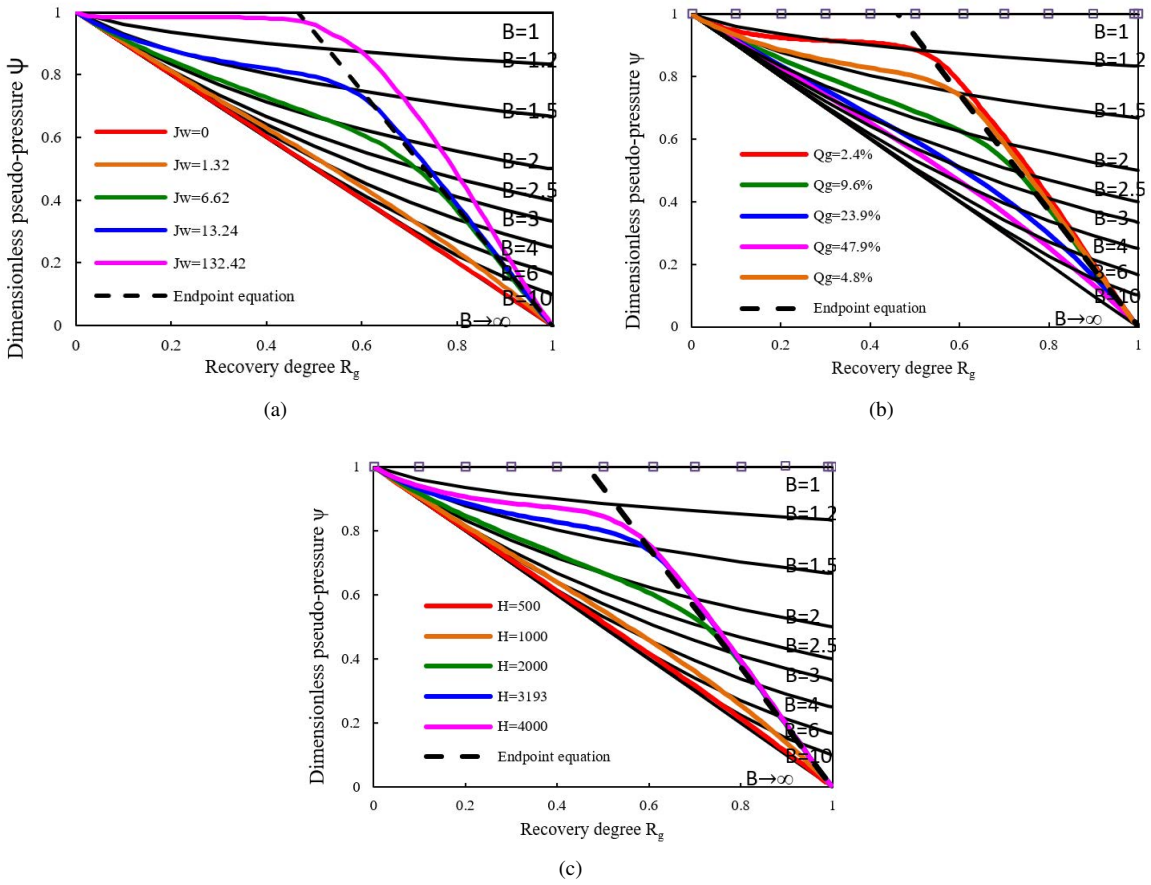

Figure 8. Dimensionless production indicator curves of the gas reservoir based on the Schithuis water invasion model under different sensitivity conditions (a) Water invasion index; (b) Gas production rate; (c) Reservoir burial depth

d) As shown in Figure 7 and Figure 8, the dimensionless production indicator curves predicted using the gas reservoir material balance equation do not completely align with the water invasion intensity indicator curves. A good fit is observed in the early upward trend stage, whereas significant deviations occur in the later downward trend stage. The best fit is achieved within the range of $1.2 < B < 2$ during the upward trend phase. Larger aquifers, lower gas production rates, and greater reservoir burial depths result in a more pronounced unsteady-state pressure depletion process, leading to a more distinct early upward trend in the production indicator curve. This, in turn, enhances its agreement with the water invasion intensity indicator curve. The agreement is found to be stronger in steady-state strong water-drive reservoirs than in unsteady-state water-drive reservoirs. Due to variations in aquifer conditions and reservoir development scenarios, the endpoint equation may differ. Thus, calibrating gas recovery or performing sensitivity analysis using a fixed endpoint curve may introduce errors.

Therefore, the method of calibrating gas recovery in water-drive gas reservoirs using the water invasion intensity indicator curve in combination with the endpoint Eq. (12) is feasible for steady-state strong water-drive reservoirs, but it results in significant errors for closed, unsteady-state water-drive reservoirs Moreover, endpoint curves are difficult to determine with precision. Consequently, gas recovery estimation based on material balance-based dynamic prediction while considering water production offers higher reliability.

The LD22-1 and LD15-1 gas fields are located in the Yinggehai Basin. The primary gas-bearing formations belong to the Ledong Formation and are mainly composed of loosely consolidated fine-grained sandstone deposited in shoreface and shallow marine environments. The reservoirs exhibit strong aquifer support and can be approximated as steady-state water-drive reservoirs. The L_2III gas reservoir in the LD22-1 gas field and the A5 well block gas

reservoir in the LD15-1 gas field are representative reservoirs of these two fields, with burial depths of approximately 1000 m and 1400 m , respectively. Both reservoirs have a similar gas production rate of approximately 6%, and no water breakthrough has been observed to date [17]. In Figure 9, the solid lines represent the actual production indicator curves of the two typical reservoirs, while the dashed lines depict the predicted production indicator curves, which were generated under the same gas production rate while considering water production based on their respective relative permeability curves. The results indicate that the production indicator curves of both reservoirs exhibit relatively good agreement with the water invasion intensity indicator curves. The actual production indicator curve of the A5 well block gas reservoir in the LD15-1 gas field is positioned higher than that of the L_2III gas reservoir in the LD22-1 gas field. Additionally, the predicted production indicator curve for the LD15-1 gas field exhibits a downward bend corresponding to a lower recovery degree (gas recovery factor) compared to the L_2III gas reservoir in the LD22-1 gas field. This finding suggests that, under the same aquifer and gas production rate conditions, water-drive gas reservoirs with shallower burial depths tend to achieve higher gas recovery.

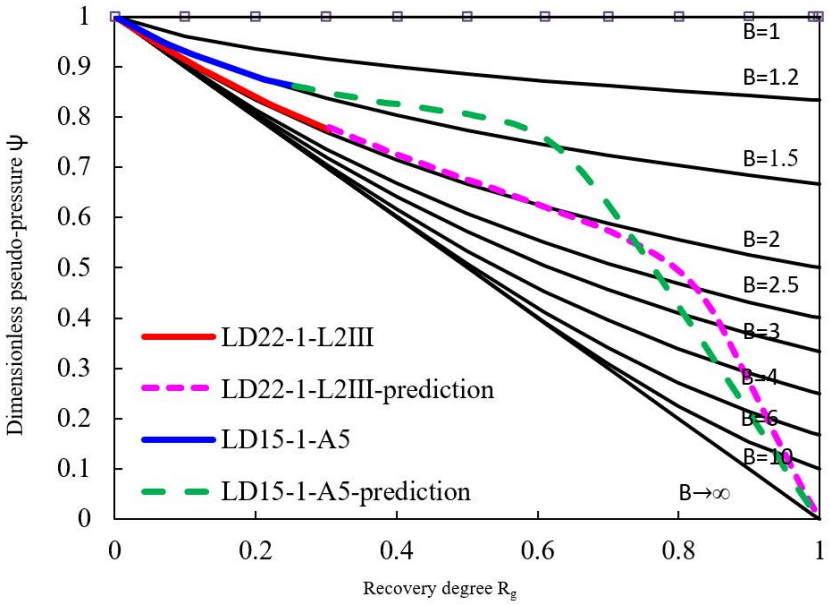

Figure 9. Dimensionless production indicator curves of typical steady-state water-drive gas reservoirs in the LD15-1 and LD22-1 gas fields [17]

3.4 Finite and Closed Aquifer Gas Reservoirs

The Yahu gas field [20], the YC13-4S gas field, and the YC13-1N gas field [14] are three finite aquifer gas reservoirs within normal pressure systems. The Anderson L gas reservoir, the NS2B gas reservoir offshore Louisiana, and the Cajun gas reservoir are three representative abnormally high-pressure gas reservoirs [4, 5, 14, 16, 21, 22]. These gas reservoirs have either been abandoned or are approaching abandonment, with extensive production histories. As shown in Figure 10, the dimensionless production indicator curves of these reservoirs consistently exhibit a smooth convex shape but demonstrate poor agreement with the water invasion intensity indicator curves. This finding confirms the limited applicability of water invasion intensity indicator curves in finite and closed aquifer gas reservoirs.

3.5 Gas Reservoirs with Variable Production Rates

As shown in Figure 11, the dimensionless production indicator curve and the gas production rate curve of a gas reservoir in the East China Sea reveal the following trends: When the gas production rate remains stable at 7%, the production indicator curve aligns closely with the water invasion intensity indicator curve. After water breakthrough, the gas production rate decreases, causing the production indicator curve to deviate upward from the water invasion intensity indicator curve. The greater the reduction in gas production rate, the more significant the upward deviation of the production indicator curve, leading to a higher abandonment pressure and lower gas recovery [13, 17]. These findings demonstrate that the applicability of the water invasion intensity indicator curve decreases when operational conditions change.

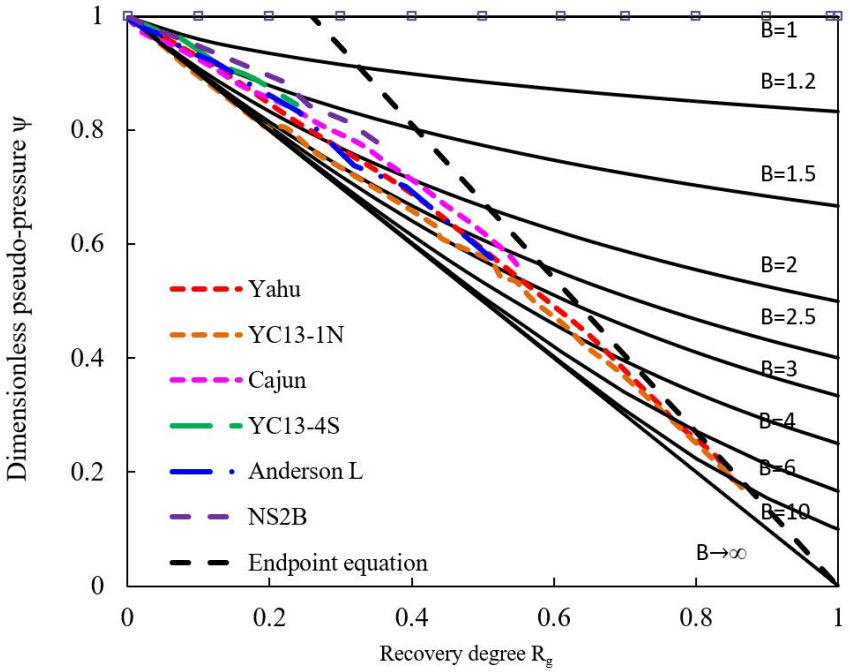

Figure 10. Dimensionless production indicator curves of typical finite and closed aquifer gas reservoirs

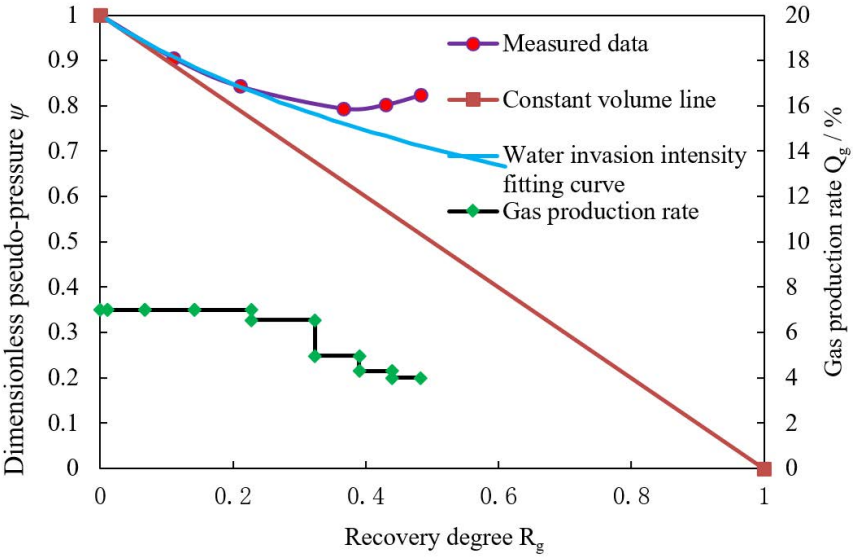

Figure 11. Dimensionless production indicator curve of the N gas reservoir in the M gas field, East China Sea [13, 17]

4 Conclusion

A reassessment of the water invasion intensity indicator curve and the endpoint equation was conducted. The water invasion intensity indicator curve is applicable only for short-term predictions in the early development stage, with better agreement observed in steady-state strong water-drive gas reservoirs. The endpoint equation may vary under different aquifer and development conditions. The classical method for gas recovery calibration shows limited applicability, and gas recovery can be estimated more reliably using a material balance-based dynamic prediction method that accounts for water production.

The traditional perspective that the production indicator curve of water-drive gas reservoirs always exhibits an upward trend was reassessed. In the early stages, the production indicator curve may exhibit an upward trend, an approximately linear segment, or a downward bend; however, it maintains an overall smooth convex shape and ultimately intersects the cumulative gas production axis at the dynamic reserves point. The larger the aquifer radii,

the higher the aquifer permeability (the greater the water invasion index), the greater the rock and formation water compressibility, the lower the gas production rate, the deeper the reservoir burial depth, the more pronounced the convex shape of the dimensionless production indicator curve, the higher the abandonment pressures, and the lower the gas recovery.

Data Availability

The data used to support the findings of this study are available from the corresponding author upon request.

Conflicts of Interest

The authors declare that they have no conflicts of interest.

References

[1] C. L. Li, *Fundamentals of Reservoir Engineering*. Beijing: Petroleum Industry Press, 2011. https://product.dangdang.com/25138249.html

[2] C. L. Li, "Theoretical study of production indicative curves from gas reservoir," *Xinjiang Petro. Geo.*, vol. 23, no. 3, pp. 236–238, 2002.

[3] L. P. Dake, *Fundamentals of Resevior Engneering*. Amsterdam. Elsevier, 1978.

[4] T. Ahmed, *Reservoir Engineering Handbook*. Beijing: Petroleum Industry Press, 2002. https://product.dangdang.com/20593644.html

[5] L. John Robert and A. Wouter Ehrenberg, *Gas Reservoir Engineering*. Beijing: Petroleum Industry Press.

[6] M. Elahmady and R. A. Wattenbarger, "A straight line p/z plot is possible in water drive gas reservoirs," in *SPE Rocky Mountain Petroleum Technology Conference/Low-Permeability Reservoirs Symposium*, 2007. https://doi.org/10.2118/103258-MS

[7] N. Ezekwe, *Petroleum Reservoir Engineering Practice*. Prentice Hall, 2010.

[8] L. Y. Zhang and J. Li, "Curve fitting method of dynamic reserve calculation in water driver gas reservoir," *Nat. Gas Ind.*, vol. 18, no. 8, pp. 26–29, 1998.

[9] S. Z. Liu, A. Y. Sun, B. G. Huang, and C. B. Xu, "The prediction method of water influx and formation pressure for a water drive gas reservoir," *Petr. Explo. Dev.*, vol. 26, no. 6, pp. 79–81, 1999.

[10] R. Y. Sheng and X. F. Li, "Influences of gas recovery rate and aquifer size on production of sandstone water-drive gas reservoirs," *Petro. Explo. Dev.*, vol. 32, no. 2, pp. 94–97, 2005.

[11] J. P. Spivy, *Gas Reservoir Engineering*. Beijing: Petroleum Industry Press, 2011.

[12] M. Li, Q. Jiang, Z. Liao, and T. Li, "Calculation method and influencing factors of water drive gas reservoir recovery," *Unconven. Oil Gas*, vol. 2, no. 1, pp. 35–40, 2015.

[13] K. F. Lu, "Applicability analysis on classical empirical relation lnw=BlnR of water invasion prediction for water drive gas reservoirs," *China Offs. Oil Gas*, vol. 28, no. 8, pp. 40–45, 2016.

[14] C. Q. Yang., X. D. Peng, X. G. Wang, J. Luo, and L. Y. Tong, "New understanding on production index curve of water drive gas reservoir: A case study of North block in YC13-1 gas field," *China Offs. Oil Gas*, vol. 29, no. 9, pp. 77–82.

[15] X. D. Peng, S. P. Zhu, Q. S. Wang, J. Luo, and Y. Lu, "A new method to calculate dynamic OGIP of gas reservoirs with restricted and closed aquifers," *China Offs. Oil Gas*, vol. 30, no. 2, pp. 77–82.

[16] X. D. Peng, C. Q. Yang, L. C. Wang, Y. Lu, and X. Liu, "New understandings of production forecast of water drive gas reservoirs," *Nat.l Gas Oil*, vol. 38, no. 3, pp. 72–78, 2020.

[17] X. D. Peng, C. Q. Yang, X. Peng, L. C. Wang, Y. Lu, X. Liu, and K. Liu, "New recognition on recovery of water drive gas reservoir: A case study of typical water drive gas reservoirs in western South China Sea," *Nat. Gas Explor. Dev.*, vol. 44, no. 2, pp. 36–43, 2021. https://doi.org/10.12055/gaskk.issn.1673-3177.2021.02.005

[18] R. G. Agarwal, R. Al-Hussainy, and J. H. J. Ramey, "The importance of water influx in gas reservoirs," *J. Petro. Tech.*, vol. 17, no. 11, pp. 1336–1342, 1965. https://doi.org/10.2118/1244-PA

[19] Y. Yang, *Fundamentals of Dynamic GIP*. Beijing: Science Press, 2016. https://www.dushu.com/book/13175187/

[20] C. Z. Peng, P. Guo, and J. F. Du, *Technology and example Analysis of Enhanced Gas Recovery in Edge/Bottom Water Gas Reservoirs*. Beijing: Petroleum Industry Press, 2015. https://product.dangdang.com/23882877.html

[21] B. P. Ramagost and F. F. Farshad, "P/Z abnormally pressured gas reservoirs." in *SPE Annual Technical Conference and Exhibition*, 1981. https://doi.org/10.2118/10125-MS

[22] R. G. Gan, "A semianalytical p/Z technique for the analysis of reservoir performance from abnormally pressured gas reservoirs," in *SPE Annual Technical Conference and Exhibition*, 2001. https://doi.org/10.2118/71514-MS